INDIVIDUAL BLADE CONTROL WITH THE SMART SPRING – A CLOSED-LOOP INDEPENDENT HARMONIC CONTROL APPROACH

Fred Nitzsche

Department of Mechanical and Aerospace Engineering
Carleton University
1125 Colonel By Drive, ME 3135, Ottawa, Ontario, Canada, K1S 5B6
E-mail: fred.nitzsche@carleton.ca

ABSTRACT

In steady-state forward flight the cyclic variation of the aerodynamic loads acting on the blade generates forces and moments that are predominantly transmitted to the fuselage at the N_b/rev harmonic of the rotor frequency, where N_b is the number of rotor blades. The Smart Spring is a semi-active device that allows actively modulating the blade pitch link axial stiffness throughout the indirect action of a piezoelectric actuator. It performs dynamic parametric excitation of the rotor system and introduces Individual Blade Control with the objective of reducing these harmonic cyclic loads transmitted to the fuselage. Previous experimental studies demonstrated that the transmissibility reduction of some harmonics could be greater than 90% for a given combination of the Smart Spring parameters. In this paper, the capability of the Smart Spring to act in the closed-loop control configuration is analytically explored for the first time. The control action results in the realization of an *independent harmonic control* of the rotor blade system, an improvement in the current state of the art of the technology. The fundamentals for the Smart Spring closed-loop independent harmonic control concept are discussed.

1 INTRODUCTION

In steady-state forward flight, the cyclic variation of the aerodynamic loads acting on the helicopter blades generate harmonic loads that are transmitted to the fuselage. The vibratory hub loads are transmitted at their nN_b/rev harmonics, where n is an arbitrary integer, N_b is the number of blades, and $1/rev$ is the fundamental frequency of the rotor. [1] These loads reduce the comfort of passengers, causes crew long-term health problems, and leads to the decrease in the fatigue life of airframe structural components.

Individual Blade Control (IBC) concept has been introduced to mitigate these loads. [2,3] However, all current IBC systems attempt to actively alter the time-varying aerodynamic loads on the blade to suppress their vibration. Successful implementation of these systems has been limited by either their complexity, or the necessity of delivering high power to the rotating system of the helicopter in a reliable manner, or else, by the electromechanical limitations of piezoelectric actuators associated with their small stroke. [4-6] All current IBC systems are based on direct active schemes that must rely in producing work against the aerodynamic forces. In direct-active schemes vibration is controlled by acting directly against the excitation force, thus requiring high actuation forces to counteract the vibratory forces. This fundamental issue is overcome by the indirect-active or semi-active schemes such as the Smart Spring that reduces vibrations by modulating the stiffness properties of the system. [7] Indirect-active systems require much lower actuation forces and displacements with respect to the direct-active schemes. The Smart Spring device allows leveraging the micro displacements produced internally by a typical piezoelectric actuator to generate actuation that can mitigate much larger external vibratory loads. The primary advantage of the IBC Smart Spring system when compared to conventional IBC systems is that it does not rely on the actuators to achieve high stroke and force simultaneously (i.e. high power). This is because the Smart Spring concept relies on delivering power not to actuate against the blade aerodynamic loads but to change the *axial spring constant* of the pitch link, which directly modifies the flexural characteristics of the blade in its torsional degree of freedom (changing its corresponding boundary condition, a basic concept that was introduced in 1994). [8] This modification, which is done continuously in time, allows the control of the aeroelastic response of the blade. The energy is redistributed in the vibration spectrum: removed from the frequencies were the rotor transmissibility to the fuselage is desired to be low (i.e. at the frequencies integer multiples of the number of blades, nN_b/rev and they immediate neighbors, $(n \pm 1)N_b/rev$ and displaced at the other frequencies, characterized for lower transmissibility from the helicopter rotor. The Smart Spring IBC concept has been extensively studied both theoretically and experimentally over the past years. [9-12] The objective of this paper, however, is to develop the mathematical basis for the closed-loop, *independent harmonic control* of the Smart Spring. This concept would enable the attenuation of the vibrations transmitted from the rotating to the non-rotating frame of the helicopter at determined harmonics without affecting the others, mainly the $1/rev$, associated with the rotor cyclic control.

2 THE SMART SPRING CONCEPT

For the sake of completeness, the Smart Spring concept is introduced. More detailed information can be found in the previous publications. [9-14] The conceptual drawing of the Smart Spring is shown in Fig. 1, where it is modeled as two mass-spring systems denoted with subscripts 1 and 2. Specifically, k_1 and m_1 represent the *primary load path* system stiffness and mass, respectively, whereas the *secondary load path* system is characterized by k_2 and m_2. The primary load path is attached to the "structure" (i.e. the blade horn) subjected to the external vibratory force induced by the blade aerodynamic loads, $F(t)$ and the "base," at which low vibration transmissibility is sought (i.e. the swashplate). There is a built-in sleeve in the main structure that is simply a conceptual representation for the Smart Spring stiffness-switching element. In its new design this action is introduced by a bi-state structure that is used to replace the two springs bonded by a friction mechanism presented in the original Smart Spring configuration.

Following this schematic, a piezoceramic stack actuator is attached to the secondary load path system, which is inserted into the sleeve.

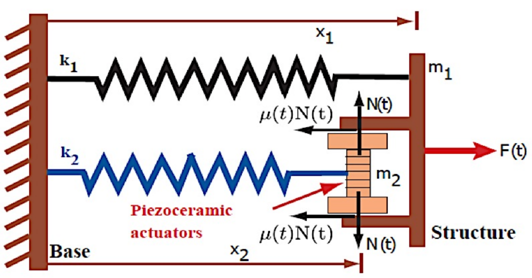

Figure 1: Fixed-base Smart Spring concept.

When the actuator is *off*, the sleeve can move freely and only the primary load path determines the transmissibility of the loads from the main structure to the Smart Spring base; the two load paths are totally decoupled. Instead, when the actuator is powered *on*, the normal force, $N(t)$ is generated and it engages the two systems: the two load path systems become fully coupled if the resultant friction force, $\mu(t)N(t)$, where $\mu(t)$ is the kinematic friction coefficient, is sufficiently large. Therefore, activating the piezoelectric actuator, the resulting stiffness of the system increases from k_1 to $k_1 + k_2$. It is worthwhile to stress once more that the present is a cartoonish representation for the Smart Spring stiffness-switching element. The basic elements of any Smart Spring are the multiple load paths and the corresponding switching devices for engaging and disengaging these load paths.

3 MATHEMATICAL MODEL OF THE SMART SPRING

The conceptual model presented in the previous section will be next used to derive the equations of the motion in the Smart Spring. The objective of the control action is to reduce the transmissibility of the dynamic loads throughout the primary load path. In the case of the shown fixed-base configuration, the external load is applied to mass m_1 and low transmissibility of that load is sought at the base of the Smart Spring.

The equations of motion for the system shown in Fig. 1 are:

$$\begin{cases} m_1\ddot{x}_1(t) + k_1 x_1(t) = F(t) \mp \mu(t)N(t) \\ m_2\ddot{x}_2(t) + k_2 x_2(t) = \pm\mu(t)N(t) \end{cases} \tag{1}$$

When the Smart Spring is *unlocked*, its two mass-spring systems are decoupled, and (1) becomes:

$$\begin{cases} m_1\ddot{x}_1(t) + k_1 x_1(t) = F(t) \\ m_2\ddot{x}_2(t) + k_2 x_2(t) = 0 \end{cases} \tag{2}$$

Therefore, the dynamic response is determined by the primary load path system (i.e. by the top equation only). When the Smart Spring is *completely locked*, the two mass-spring systems move in unison and, thus, their displacements (and accelerations) are identical, $x_1 \equiv x_2$. In this case, the summation of the two equations in (1) reduces to:

$$(m_1 + m_2)\,\ddot{x}_1(t) + (k_1 + k_2)\,x_1(t) = F(t) \tag{3}$$

However, in the *general case*, the summation of the two equations in (1) yields:

$$m(t)\ddot{x}_1(t) + k(t)x_1(t) = F(t) \tag{4}$$

where:

$$\begin{aligned} m(t) &= m_1\left(1 + \frac{m_2}{m_1}\frac{\ddot{x}_2(t)}{\ddot{x}_1(t)}\right) \\ k(t) &= k_1\left(1 + \frac{k_2}{k_1}\frac{x_2(t)}{x_1(t)}\right) \end{aligned} \tag{5}$$

Taking into consideration that the mass of the secondary path in the Smart Spring, m_2 is negligible with respect to the mass of the main structure, m_1 (i.e. the blade), $|m_2\ddot{x}_2(t)| \ll |m_1\ddot{x}_1(t)|$, and the Smart Spring turns out to be a stiffness modulation device that performs *parametric excitation* of the system:

(6) $$m_1\ddot{x}_1(t) + k(t)x_1(t) = F(t)$$

4 FREQUENCY DOMAIN MATHEMATICAL MODEL AND ITS ANALYTICAL SOLUTION

The mathematical model is solved in the frequency domain using the harmonic balance method, assuming that the solution should also be harmonic on the exciting harmonic frequencies. It can be proved that the Smart Spring transmissibility characteristics at a certain frequency depends only on two dimensionless design parameters: the stiffness ratio between the primary and secondary systems and the natural frequency associated with the primary system besides its operational parameters: the control frequency and phase.

4.1 The Smart Spring control function

It has been determined in the previous section that only the stiffness of the Smart Spring system is a function of time and that it involves (1) the ratio between the displacements of the secondary and primary path systems and (2) the spring constants associated with the primary and secondary paths (5). The control function that modulates this ratio from the value of the main spring k_1 to the value of the coupled system, $k = k_1 + k_2$, is now introduced. The control function model depends fundamentally on the design of the switching mechanism of the Smart Spring. In the cartoonish Smart Spring operation scheme presented in this paper a friction-based mechanism is represented. In a previous work this system was numerically simulated by a typical representation of the dry (Coulomb) friction effect where the *dynamic friction coefficient*, $\mu(t)$ was a function of the material and the absolute value of the relative speed between the two elements of the sleeve, $|\dot{x}_1 - \dot{x}_2|$. [10] In these time-domain simulations that were supported by experimental verifications, [11,12] it was determined that if both the applied piezoelectric normal force and the piezoelectric stroke are sufficient large to guarantee perfect locking and unlocking between the primary and the secondary load paths during the operation of the Smart Spring, the square wave is a good approximation for the switching process. This is equivalent to following an *on-off control law*. Hence, the square-wave control function shown in Fig. 2 is considered to perform such a modulation of the stiffness by the Smart Spring in this work. When the control function, $f(\alpha) = x_2/x_1$ is equal to 0 (or 1), the stiffness of the system assumes the value of k_1 (or $k = k_1 + k_2$), as it can be verified from (5). However, the locking and unlocking of the switching mechanism has been verified in experiments to be a concern in the design of the switching element, thereof requiring the necessary attention in the selection of the piezoelectric material and stacking procedure. [11] For this reason, in its new version, the Smart Spring switching mechanism was changed to a bi-state smart structure that does not rely on friction for its operation. However, the mathematical model represented by (6) and the following are still appropriate.

The time dependence of the control function is introduced by a dimensionless angular parameter:

(7) $$\alpha = r\psi + \phi$$

so that the system stiffness in the frequency domain is modulated as $k(\alpha) = k_1 + k_2 f(\alpha)$, where $\psi = \Omega t$ is the non-dimensional time (blade azimuth angle), Ω the reference frequency (the fundamental rotor frequency) and ϕ the control phase angle (control delay from a reference azimuth value). In (7), the parameter $r = \omega_c/\Omega$ represents the harmonic number of the fundamental frequency, Ω targeted for the control action (i.e. N_b/rev), where ω_c is the control frequency.

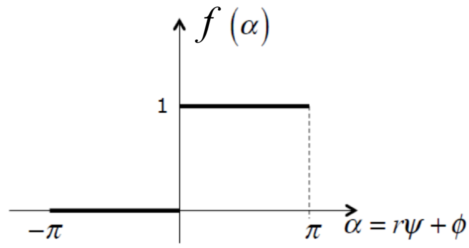

Figure 2: Smart Spring control function.

4.2 Closed mathematical solution by the harmonic balance method

The harmonic balance method is the basis for the mathematical model of the Smart Spring in the frequency domain. It allows the study of the response of the system in terms of its harmonic components and it was derived in a previous work. [13] It is summarized in this section for the sake of completeness.

The following complex Fourier series representations for the exciting force and for the response of the primary load path system, respectively, are assumed:

(8) $$F(t) = \sum_{n=-\infty}^{+\infty} F_n e^{in\psi}; \quad x_1(t) = \sum_{n=-\infty}^{+\infty} x_{1_n} e^{in\psi}$$

where $n = \omega/\Omega$ is any harmonic of interest of the fundamental rotor frequency. The square-wave control function can be likewise represented in complex Fourier series:

(9) $$f(\alpha) = \frac{1}{2} + \frac{1}{i\pi} \sum_{p=\pm1,\pm3,\ldots}^{+\infty} \frac{1}{p} e^{ip\alpha}$$

where p is any integer number. Hence:

$$k(\alpha) = k_0 + \frac{k_2}{i\pi} \sum_{p=\pm1,\pm3,\dots}^{+\infty} \frac{1}{p} e^{ip\alpha} \tag{10}$$

where $k_0 = (2k_1 + k_2)/2$ is the average value of the Smart Spring stiffness in time, according to Fig. 3:

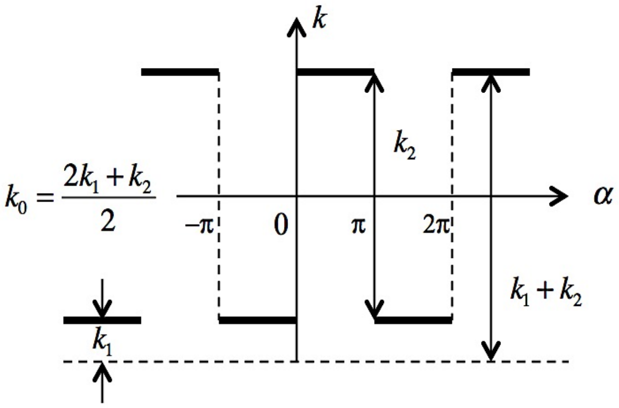

Figure 3: Smart Spring stiffness modulation in time.

Using (8) and (10) into (6), the equation of motion for the Smart Spring can be converted into the frequency domain:

$$\begin{aligned} & -m_1\Omega^2 \sum_{n=\pm1,\pm2,\dots}^{+\infty} n^2 x_{1_n} e^{in\psi} \\ & + \left[k_0 + \frac{k_2}{i\pi} \sum_{p=\pm1,\pm3,\dots}^{+\infty} \frac{1}{p} e^{ip\alpha}\right] \\ & \cdot \left[x_{1_0} + \sum_{n=\pm1,\pm2,\dots}^{+\infty} x_{1_n} e^{in\psi}\right] \\ & = F_0 + \sum_{n=\pm1,\pm2,\dots}^{+\infty} F_n e^{in\psi} \end{aligned} \tag{11}$$

where x_{1_0} represents the new equilibrium position of the primary load path due to the operation of the Smart Spring, that is slightly changed from its static value, F_0/k_1.

Using (7) and the identity $1/i = e^{-i\pi/2}$, (11) can be rewritten as:

$$\begin{aligned} & \sum_{n=-\infty}^{+\infty} \sum_{p=\pm1,\pm3,\dots}^{+\infty} \Big[\left(-m_1\Omega^2 n^2 + k_0\right) x_{1_n} e^{in\psi} + \\ & + \frac{k_2}{\pi}\frac{1}{p} x_{1_n} e^{i(pr+n)} e^{i(p\phi - \frac{\pi}{2})}\Big] = \\ & = \sum_{n=-\infty}^{+\infty} F_n e^{in\psi} \end{aligned} \tag{12}$$

Because both p and n are dummy indices, noting that $(pr + n) \to \pm\infty$ as $n \to \pm\infty$ and $p \to \pm\infty$, the following transformation applies:

$$\begin{aligned} & \sum_{n=-\infty}^{+\infty} \sum_{p=\pm1,\pm3,\cdots}^{+\infty} x_{1_n} e^{i(pr+n)\psi} = \\ & = \sum_{n=-\infty}^{+\infty} \sum_{p=\pm1,\pm3,\cdots}^{+\infty} x_{1_{(pr+n)}} e^{in\psi} \end{aligned} \tag{13}$$

Equation (13) allows that (12) can be reduced to:

$$\begin{aligned} & \sum_{n=-\infty}^{+\infty} \sum_{p=\pm1,\pm3,\dots}^{+\infty} \Big[\left(-m_1\Omega^2 n^2 + k_0\right) x_{1_n} + \\ & + \frac{k_2}{p\pi} x_{1_{(pr+n)}} e^{i(p\phi - \frac{\pi}{2})}\Big] e^{in\psi} = \\ & = \sum_{n=-\infty}^{+\infty} F_n e^{in\psi} \end{aligned} \tag{14}$$

that corresponds to an infinite set of Complex Frequency Response Functions (CFRF):

$$\begin{aligned} & \left(-m_1\Omega^2 n^2 + k_0\right) x_{1_n} + \\ & + \frac{k_2}{\pi} \sum_{p=\pm1,\pm3,\dots}^{+\infty} \frac{1}{p} e^{i(p\phi - \frac{\pi}{2})} x_{1_{(pr+n)}} = F_n \end{aligned} \tag{15}$$

for $n = 0, \pm1, \pm2, \cdots$. The CFRFs relate every harmonic of F_n to the corresponding harmonic of x_{1_n}.

It is convenient to obtain the non-dimensional form of (15) by dividing the expression by k_1, the primary path stiffness. Noticing that the natural frequency of the primary load path is given by $\omega_1 = \sqrt{k_1/m_1}$ and introducing the dimensionless parameter $\kappa = k_2/k_1$ one obtains:

$$\begin{aligned} & \left[-\left(\frac{\Omega}{\omega_1}\right)^2 n^2 + 1 + \frac{\kappa}{2}\right] x_{1_n} + \\ & + \frac{\kappa}{\pi} \sum_{p=\pm1,\pm3,\dots}^{+\infty} \frac{1}{p} e^{i(p\phi - \frac{\pi}{2})} x_{1_{(pr+n)}} = \frac{F_n}{k_1} \end{aligned} \tag{16}$$

It is important to understand the physical meaning of (16). The summation appearing in the second term of (16) is related to the Smart Spring control function. Because the control function is a square wave, the amplitude of the harmonics decrease as the inverse of p, meaning that the harmonics more distant from the target (controlled) harmonic, r will be lesser affected by the Smart Spring operation. More importantly, this is the only term that is dependent on the control phase angle, ϕ

and it represents the coupling among the harmonics introduced by the operation of the Smart Spring. As such, this term is also responsible for the spreading in the spectrum of the vibration energy, away from the targeted frequency for control, and ultimately the control objective. Without this effect, the Smart Spring control is represented by the first term of (16):

$$\left[-\left(\frac{\Omega}{\omega_1}\right)^2 n^2+1+\frac{\kappa}{2}\right]x_{1_n}\cdot=\frac{F_n}{k_1} \tag{17}$$

4.3 Simplified solution – understanding the physics of the Smart Spring operation

The over-simplified situation represented by (17) is explored in this Section only for the sake of better understanding the physics involved in the Smart Spring operation. Rearranging this expression:

$$\left(1-\left(\frac{\Omega}{\omega_1}\right)^2 n^2\right)\left[1+\frac{\kappa}{2}\left(1-\left(\frac{\Omega}{\omega_1}\right)^2 n^2\right)^{-1}\right]x_{1_n}=\frac{F_n}{k_1} \tag{18}$$

and observing that:

$$G_0(n)=\left(1-\left(\frac{\Omega}{\omega_1}\right)^2 n^2\right)^{-1}=\frac{\omega_1^2}{\omega_1^2-\omega^2} \tag{19}$$

is the usual Frequency Response Function (FRF) of an undamped single-degree-of-freedom system, (18) can be written as:

$$G_0^{-1}(n)\left[1+\frac{\kappa}{2}G_0(n)\right]x_{1_n}=\frac{F_n}{k_1} \tag{20}$$

Solving for x_{1_n}:

$$\frac{x_{1_n}}{F_n/k_1}=G(n,\kappa)=\frac{G_0(n)}{1+\frac{\kappa}{2}G_0(n)} \tag{21}$$

Equation (21) can now be identified to the unit feedback closed-loop system shown in in Fig. 4, for which the open-loop transfer function is $G_0(n)$ and the gain is $\kappa/2$ (one-half the ratio between the secondary and primary spring constants in the Smart Spring). This means that when the loop is open, $\kappa=0$ (i.e. when $k_2=0$ and the secondary system is unlocked) and the Smart Spring acts as filter for the axial loads acting on the primary path.

If m_1 and k_1 are respectively identified as the effective inertia of the blade in pitch and the stiffness of the pitch link, $\omega_1=\sqrt{k_1/m_1}$ is approximately the natural frequency of the rigid body pitch mode of the blade. Then, when the Smart Spring *is not* operating the harmonic components of $F(t)$ are fully transmitted to the swashplate, either dynamically attenuated or amplified according to the open-loop FRF, $G_0(n)$. However, when the Smart Spring is operating and the stiffness of the pitch link is modulated in time, these harmonics shall be further attenuated according to the fundamental principle of the closed-loop regulators. This attenuation is given by the closed-loop transfer function, $G(n,\kappa)$.

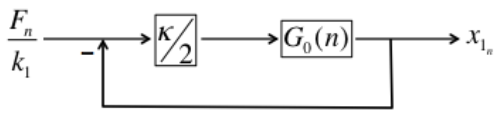

Figure 4: Characteristic Single-input, single output (SISO) feedback closed-loop control action introduced by the Smart Spring operation on individual harmonics of the external loads neglecting the square-wave control function.

4.4 Rigorous solution – the influence of the Smart Spring control function

In this Section, the summation in the second term of (16) is explicitly developed for $p_{max}=\pm 5$ that includes the most affected harmonics introduced by the control function of the Smart Spring:

$$\begin{aligned}\sum_{p=\pm1,\pm3,\dots}^{+\infty}\frac{1}{p}e^{i(p\phi-\frac{\pi}{2})}=\dots&-\frac{1}{5}e^{i(-5\phi-\frac{\pi}{2})}x_{1_{-5r+n}}+\\&-\frac{1}{3}e^{i(-3\phi-\frac{\pi}{2})}x_{1_{-3r+n}}+\\&-e^{i(-\phi-\frac{\pi}{2})}x_{1_{-r+n}}+\\&+e^{i(\phi-\frac{\pi}{2})}x_{1_{r+n}}+\\&+\frac{1}{3}e^{i(3\phi-\frac{\pi}{2})}x_{1_{3r+n}}+\\&+\frac{1}{5}e^{i(5\phi-\frac{\pi}{2})}x_{1_{5r+n}}+\dots\end{aligned} \tag{22}$$

Introducing Euler's formula, $e^{i\theta}=\cos\theta+i\sin\theta$ in (22), considering the real and imaginary parts of each harmonic present, the CFRFs between the real and imaginary parts of the harmonics x_{1_n} and their corresponding counterparts originated from exciting force, F_n are obtained:

$$\begin{aligned}&\left[-\left(\frac{\Omega}{\omega_1}\right)^2 n^2+1+\frac{\kappa}{2}\right]\left[\mathrm{Re}(x_{1_n})+i\,\mathrm{Im}(x_{1_n})\right]+\frac{2\kappa}{\pi}\Big[\dots+\\&+\frac{1}{5}cos(5\phi)\,\mathrm{Im}(x_{1_{5r+n}})+\frac{1}{5}sin(5\phi)\,\mathrm{Re}(x_{1_{5r+n}})+\\&+\frac{1}{3}cos(3\phi)\,\mathrm{Im}(x_{1_{3r+n}})+\frac{1}{3}sin(3\phi)\,\mathrm{Re}(x_{1_{3r+n}})+\\&+cos(\phi)\,\mathrm{Im}(x_{1_{r+n}})+sin(\phi)\,\mathrm{Re}(x_{1_{r+n}})\Big]=\\&=\frac{1}{k_1}\left[\mathrm{Re}(F_n)+i\,\mathrm{Im}(F_n)\right]\end{aligned} \tag{23}$$

Equation (23) is conveniently expressed in matrix form, which allows for the solution of all harmonics of x_{1_n} as a function of any given exciting frequency spectrum when the Smart Spring is operating:

$$\mathbf{A}(n)\mathbf{x}_1(n) = \mathbf{F}(n) \tag{24}$$

for $n = 0, \pm 1, \pm 2, \ldots, \pm\infty$.

If $N = n + rp_{max}$, $\mathbf{x}_1(n)$ and $\mathbf{F}(n)$ are vectors of dimension $2N$. They collect the real and the imaginary parts of the harmonics of x_{1_n} and F_n, respectively in their upper and lower halves, as shown in (25):

$$\mathbf{x}_1(n) = \begin{Bmatrix} \vdots \\ \mathrm{Re}\left(x_{1_{n+1}}\right) \\ \mathrm{Re}\left(x_{1_n}\right) \\ \mathrm{Im}\left(x_{1_n}\right) \\ \mathrm{Im}\left(x_{1_{n+1}}\right) \\ \vdots \end{Bmatrix}; \quad \mathbf{F}(n) = \frac{1}{k_1}\begin{Bmatrix} \vdots \\ \mathrm{Re}\left(F_{n+1}\right) \\ \mathrm{Re}\left(F_n\right) \\ \mathrm{Im}\left(F_n\right) \\ \mathrm{Im}\left(F_{n+1}\right) \\ \vdots \end{Bmatrix} \tag{25}$$

and $\mathbf{A}(n)$ is the square matrix of dimension $2N$:

$$\mathbf{A}(n) = \left(1 + \frac{\kappa}{2}\right)\mathbf{I} - \left(\frac{\Omega}{\omega_1}\right)^2 \grave{\mathbf{n}}^2 + \frac{2\kappa}{\pi}\mathbf{B}(n) \tag{26}$$

where $\mathbf{I}$ is the identity matrix and $\grave{\mathbf{n}}$ is the diagonal matrix collecting the harmonic numbers (the grave accent denotes diagonal matrices in the present paper), as follows:

$$\grave{\mathbf{n}} = \begin{bmatrix} \ddots & & & & & \\ & n+1 & & & & \\ & & n & & & \\ & & & n & & \\ & & & & n+1 & \\ & & & & & \ddots \end{bmatrix} \tag{27}$$

Also in (26):

$$\mathbf{B}(n) = \begin{bmatrix} \mathbf{B}_{11}(n) & \mathbf{B}_{12}(n) \\ \mathbf{0} & \mathbf{0} \end{bmatrix} \tag{28}$$

where $\mathbf{0}$ is the null matrix. In (28), $\mathbf{B}_{11}(n)$ and $\mathbf{B}_{12}(n)$ are sparse but full square matrices of dimension N, dependent on both the controlled harmonic, r and the control phase, ϕ. They follow the multiple diagonal structure discussed in the Appendix.

5 OPEN-LOOP NUMERICAL SIMULATIONS

The mathematical model derived in Section 4.4 was fully implemented in previous works to analyze the harmonic response of the fixed-base and the based-excited Smart Spring configurations. [13,14] The open-loop harmonic response was calculated for different values of Ω/ω_1 as a function of κ and ϕ. A flat unitary spectrum for the excitation force was considered in the simulations, $k_1\mathbf{F}(n) = \lfloor \cdots, 1, 1, 1, \cdots \rfloor^T$ and then (24) was solved for $\mathbf{x}_1(n)$.

In Fig. 5, a sample result from these parametric studies is shown. In particular, the normalized magnitude plots for the harmonics n = 3, 4 and 5 of the primary path dynamic response with respect their corresponding uncontrolled case are exhibited for two values of the Smart Spring design parameter: $\Omega/\omega_1 > 1$ and $\Omega/\omega_1 < 1$. The control frequency is set at r = 4 (i.e. at the 4th harmonic of the rotor fundamental frequency, or $4/rev$, aiming at dynamic loads reduction of a 4-bladed rotor).

In these plots both the relative stiffness between the secondary and primary paths (the closed-loop control gain, κ) and the Smart Spring control phase angle, ϕ are varied. It is verified that substantial reductions in the transmissibility, notably at the harmonic targeted for the control occur if the "right" combination of the Smart Spring parameters is chosen. Significantly higher reductions were verified in general for $\omega_1 > \Omega$. However, it is also seen that ample spillover happens at harmonics not targeted by the control action. High sensitivity of the response to the control and design parameters is noticeable, producing amplification of the transmissibility at harmonics that should targeted for rotor-induced vibration control as well, such as $3/rev$ and $5/rev$.

This behavior was supported by experimental work conducted with a scaled helicopter blade model, from which one result is depicted in Fig. 6. [11,12] It should be noted, however, that there is no direct relation between the simulated cases and the tested cases to support a quantitative validation of the model. This is due to the different excitation spectrum used in the experimental tests. These were performed in a whirl tower with a single blade rotor using a fan placed underneath the apparatus to excite the blade. [11,12] However, it is clear from the results that the sinusoidal variation of the dynamic response with the control phase angle is observed both in the test and the simulation results.

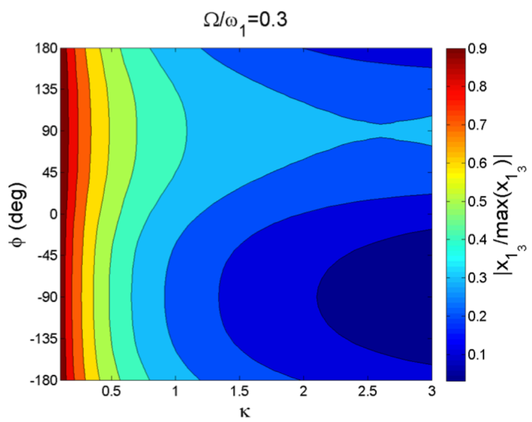

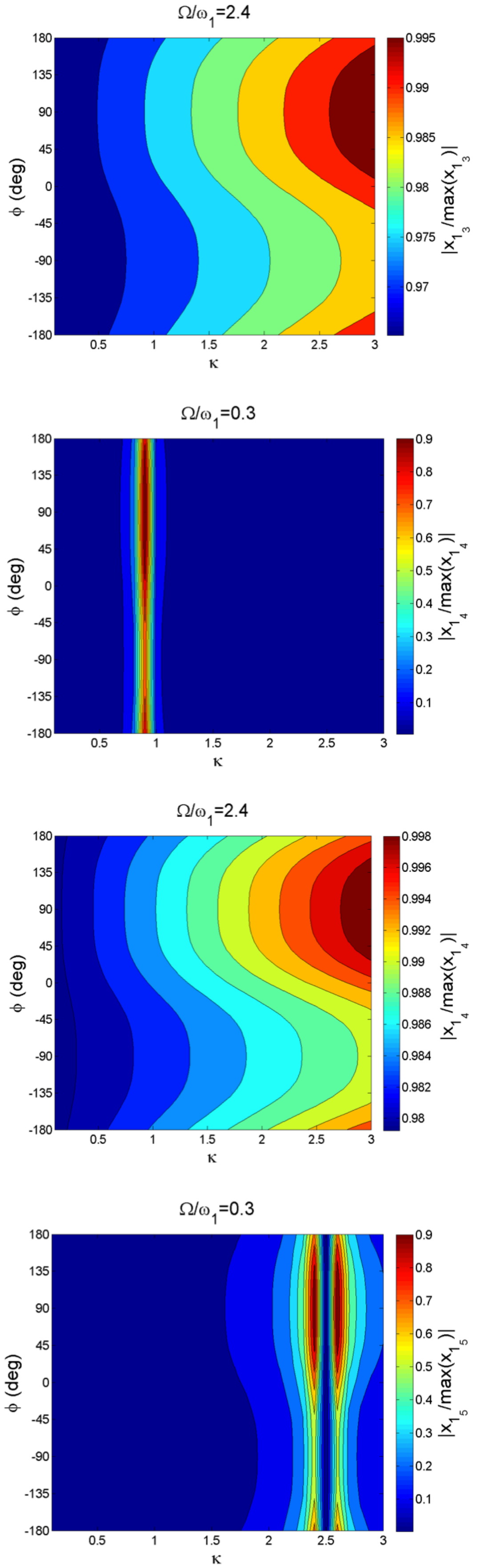

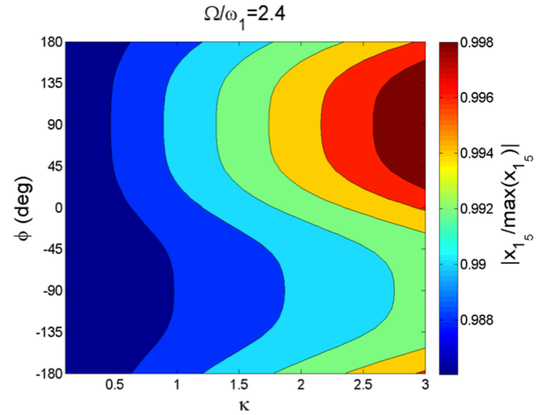

Figure 5: Open-loop parametric simulations: normalized magnitudes of the 3rd to 5th harmonics of the fundamental rotor frequency when the Smart Spring is operating at the 4th harmonic. Results for two different values of the Smart Spring design parameter Ω/ω_1 and for different gains and control phases. [13,14]

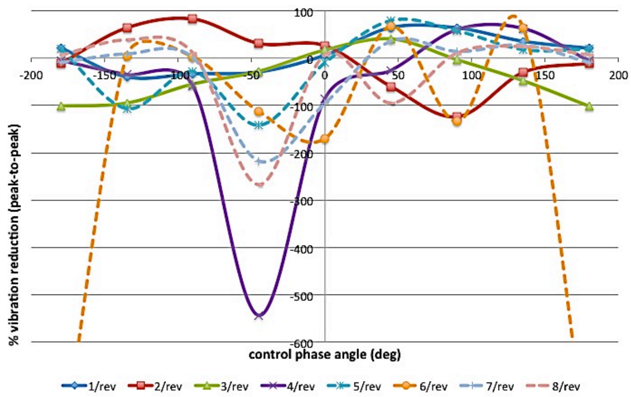

Figure 6: Open-loop experimental results for Smart Spring transmissibility control of the peak-to-peak levels obtained with a 1-blade rotor. The control frequency set at 2/rev with variable control phase angle. Results are shown for the first 8 harmonics of the rotor fundamental frequency (negative values represent vibration amplification with respect to the baseline value). [11,12]

6 INDEPENDENT HARMONIC CONTROL OF THE SMART SPRING

All the previous results indicate that a closed-loop action that provides a "right" combination of the Smart Spring parameters should be sought to guarantee continuous reduction in the transmissibility of the target controlled harmonic without producing significant spillover at other important harmonics for rotor vibration control. In this Section the fundamentals for the closed-loop independent harmonic control of the Smart Spring will be identified.

6.1 Closing the loop

Starting from (26), this expression is rearranged as:

$$\mathbf{A}(n) = \left(\mathbf{I} - \left(\frac{\Omega}{\omega_1}\right)^2 \text{`}\mathbf{n}^2\right) + \frac{\kappa}{2}\left(\mathbf{I} + \frac{4}{\pi}\mathbf{B}(n)\right) \tag{29}$$

The first term is factored out to produce:

$$\mathbf{A}(n) = \left(\mathbf{I} - \left(\frac{\Omega}{\omega_1}\right)^2 \text{`}\mathbf{n}^2\right)\left(\mathbf{I} + \frac{\kappa}{2}\left(\mathbf{I} - \left(\frac{\Omega}{\omega_1}\right)^2 \text{`}\mathbf{n}^2\right)^{-1}\left(\mathbf{I} + \frac{4}{\pi}\mathbf{B}(n)\right)\right) \tag{30}$$

Similarly to Section 4.3, the first term is now identified to the open-loop transfer *matrix*:

$$\mathbf{G}_0^{-1}(n) = \mathbf{I} - \left(\frac{\Omega}{\omega_1}\right)^2 \text{`}\mathbf{n}^2 \tag{31}$$

which is notable *diagonal*. This yields for (30):

$$\mathbf{A}(n) = \mathbf{G}_0^{-1}(n)\left(\mathbf{I} + \frac{\kappa}{2}\mathbf{G}_0(n)\left(\mathbf{I} + \frac{4}{\pi}\mathbf{B}(n)\right)\right) \tag{32}$$

Using the latter result into (24) and solving for $\mathbf{x_1}(n)$:

$$\mathbf{x_1}(n) = \left(\mathbf{I} + \frac{\kappa}{2}\mathbf{G}_0(n)\left(\mathbf{I} + \frac{4}{\pi}\mathbf{B}(n)\right)\right)^{-1}\mathbf{G}_0(n)\frac{1}{k_1}\mathbf{F}(n) \tag{33}$$

Recognizing that $\mathbf{B}(n)$ is also a function of the control frequency and phase introduced by the control function of the Smart Spring, the feedback matrix is now defined:

$$\mathbf{H}(n;r,\phi) = \mathbf{I} + \frac{4}{\pi}\mathbf{B}(n;r,\phi) \tag{34}$$

Equation (33) is then simplified to:

$$\mathbf{x_1}(n) = \left(\mathbf{I} + \frac{\kappa}{2}\mathbf{G}_0(n)\mathbf{H}(n;r,\phi)\right)^{-1}\mathbf{G}_0(n)\frac{1}{k_1}\mathbf{F}(n) \tag{35}$$

Equation (35) can be directly identified to the closed-loop transfer *matrix*, $\mathbf{G}(n;\kappa,r,\phi)$ of the feedback system depicted in Fig. 7 that relates the harmonics of x_{1_n} to the harmonics of the excitation spectrum, F_n: [15]

$$\mathbf{x_1}(n) = \mathbf{G}(n;\kappa,r,\phi)\frac{1}{k_1}\mathbf{F}(n) \tag{36}$$

where closed-loop matrix is:

$$\mathbf{G}(n;\kappa,r,\phi) = \left(\mathbf{I} + \frac{\kappa}{2}\mathbf{G}_0(n)\mathbf{H}(n;r,\phi)\right)^{-1}\mathbf{G}_0(n) \tag{37}$$

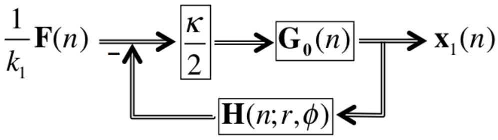

Figure 7: Multiple-input, multiple-output (MIMO) feedback closed-loop control system characterizing the Smart Spring operation.

6.2 Closed-loop IBC for the Smart Spring independent harmonic control

From the previous Section, it can be seen that the design of the Smart Spring closed-loop control is based on a simple and conventional feedback control system. The spillover coupling effect introduced by the Smart Spring control function is represented by the feedback matrix transfer function $\mathbf{H}$ (in the feedback branch of the control loop), which in a conventional feedback control theory plays the role of a *sensor system*. This matrix is, as indicated in the Appendix, a sparse but *full matrix* whose structure is dependent on the controlled harmonic number, r and the control angle, ϕ. As such, this matrix is in the present case the only component of the closed-loop system responsible for the coupling among the harmonics introduced by the operation of the Smart Spring. If this matrix were diagonal, the multiple-input multiple-output (MIMO) feedback system would collapse into a *collection of independent* single-input single-output feedback systems (SISOs) relating the harmonics x_{1_n} to the corresponding harmonics of the excitation spectrum, F_n; every SISO system resembling to the one depicted in Fig. 4. Therefore, the objective of achieving an *independent harmonic control* using the Smart Spring falls into the task of *diagonalizing* the matrix $\mathbf{H}(n;r,\phi)$. This is equivalent to determine the *linear transformation of generalized coordinates* that is able to decouple the system. The original (physical) generalized coordinates are associated with the harmonic components of the response, x_{1_n}. The new coordinates will be a *linear combination* of these harmonic components. The process is identical to decoupling any linear multi-degree-of-freedom dynamic system into its natural modes of vibration by solving the eigenvalue problem associated with the dynamic matrix of that system. By analogy, in the present case, the dynamic matrix is the feedback matrix $\mathbf{H}(n;r,\phi)$. Then, the following identity holds: [16]

$$\mathbf{HU} \equiv \mathbf{U}\text{`}\mathbf{V} \Rightarrow \text{`}\mathbf{V} = \mathbf{U}^{-1}\mathbf{HU} \tag{38}$$

where $\mathbf{U}$ is the *modal matrix* associated with $\mathbf{H}$ (i.e. collecting the eigenvectors of $\mathbf{H}$ along its columns) and $\text{`}\mathbf{V}$ is the *spectral matrix* associated with $\mathbf{H}$ (i.e collecting the corresponding eigenvalues of $\mathbf{H}$ along its diagonal). Using this transformation (37) yields:

$$\grave{\mathbf{G}}(n;\kappa,r,\phi)=\left(\mathbf{I}+\frac{\kappa}{2}\mathbf{G}_0(n)\grave{\mathbf{V}}(n;r,\phi)\right)^{-1}\mathbf{G}_0(n) \tag{39}$$

where the closed-loop transfer matrix is now *diagonal*. It is worthwhile to mention that the gain of each individual harmonic component in the independent harmonic control situation is fully determined by the eigenvalues of $\mathbf{H}$, as indicated in (39). These are also a function of the control harmonic number, r and the control phase angle, ϕ following the matrix $\mathbf{H}$ structure.

Realization of this independent harmonic control system physically requires the introduction of a frequency analyzer in the feedback loop that reads from the Smart Spring primary path the transmitted signal harmonic components and performs a combination of these components according to the pre-established eigenvectors of $\mathbf{H}$ (Fig. 8).

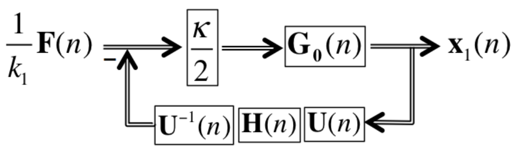

Figure 8: Realization of the independent harmonic control using the Smart Spring IBC concept.

7 CONCLUSIONS

The present work developed the individual blade closed-loop control approach for the Smart Spring device in the frequency domain using the harmonic balance method. The closed mathematical solution for this feedback control system was derived. The fundamentals of an independent control for the harmonics of the vibration spectrum transmitted through the pitch link from the rotating to the non-rotating frame using the Smart Spring were established. The basis for the realization of this new concept in practical systems was discussed.

REFERENCES

[1] Johnson, W., *Helicopter Theory*, Dover Publications, 1994.

[2] Kretz, M., "Research on Multicyclic and Active Control of Rotary Wings," *Vertica*, Vol. 1, No. 1/2, pp. 95-105, 1976.

[3] Ham, N. D., "Helicopter Individual Blade Control at MIT 1977-1985, *Vertica,* Vol. 11, No. 1/2, pp. 109-122, 1987.

[4] Jacklin, S. A., Haber, A., de Simone, G., Norman, T. R., Kitaplioglu, C., and Shinoda, P., Full-scale wind tunnel test of an individual blade control system for a UH-60 helicopter, *Proc.* American Helicopter Society 58th International Annual Forum, Montreal, Canada, 2002.

[5] Koratkar, N. A. and Chopra, I., Open-loop hover and wind tunnel testing of Mach-scaled rotor with trailing- edge flaps, *Proc.* 42nd AIAA/ ASME/ASCE/AHS/ASC Structures, Structural Dynamics and Exhibit Technical Papers, Seattle, WA, pp. 1317-1331, 2001.

[6] Roth, D., Enenkl, B., and Dieterich, O., Active rotor control by flaps for vibration reduction-full scale demonstrator and first flight test results. *Proc.* 32nd European Rotorcraft Forum, Maastricht, The Netherlands, pp.801-814, 2007

[7] Nitzsche, F., Grewal, A., and Zimcik, D. G., *Structural component having means for cyclically varying its stiffness to control vibrations - Smart Spring*. Patents: 1999 USA (5,973,440), 2001 European Community (EP-996570-B1), and Canada (2,242,214).

[8] Nitzsche, F., Lammering, R., and Breitbach, E. J., "Can Smart Materials Modify Blade Root Boundary Conditions to Attenuate Helicopter Vibration?" *Proc.* 4th International Conference on Adaptive Structures, Cologne, Germany, November 2-4, 1993, E. Breitbach, B. K. Wada and M. Natori, Editors, Technomic, Lancaster, PA, pp. 139-150, 1994.

[9] Yong, C., Zimcik D. G., Wickramasinghe, V. K. and Nitzsche, F., "Development of the Smart Spring for Active Vibration Control of Helicopter Blades", *Journal of Intelligent Material Systems and Structures*, Vol. 15, pp. 37-47, 2004.

[10] Wickramasinghe, V. K., Yong, C., Zimcik D. G., Harold T., and Nitzsche, F., "Smart Spring: A Novel Impedance Control Approach for Active Vibration Suppression Applications", *Proc.* SPIE, Smart Structures and Materials 2004: Smart Structures and Integrated Systems, Vol. 5390, 2004.

[11] Nitzsche, F., Feszty, D., Grappasonni, C., and Coppotelli, G., "Whirl-tower Open Loop Experiments and Simulations with an Adaptive Pitch Link Device for Helicopter Rotor Vibration." *Proc.* 54th AIAA/ASME/ASCE/AHS/ ASC Structures, Structural Dynamics and Materials Conference, Paper No. AIAA-2013-1711, Boston, MA, April 8-11, 2013.

[12] Nitzsche, F. et al, "Developments on the Hybrid Stiffness - Flow Control Active System for Rotor Vibration Attenuation Project – SHARCS," Paper No. 010. *Proc.* 38th European Rotorcraft Forum, Amsterdam, The Netherlands. September 4-7, 2012.

[13] Nitzsche, F., Arras, M., and Coppotelli, G., "Closed-Loop Control of the Smart Spring – An Analytical Solution for the Actuator Model," *Proc.* VIII ECCOMAS Thematic Conference on Smart Structures and Materials (SMART 2017), Paper No. 40, Madrid, Spain, 5-8 June, 2017.

[14] Nitzsche, F., Arras, M., and Coppotelli, G.,

"Frequency-domain Mathematical Model of the Smart Spring Device for Vibration Reduction," *Proc.* 26th International Conference on Adaptive Structures and Technologies (ICAST 2015), Paper No. 26, October 14-16, Kobe, Japan, 2015.

[15] Ogata, K., *Modern Control Engineering,* 1st Edition, Prentice-hall, Englewood Cliffs, NJ, 1970, pp. 688-690.

[16] Strang, G., *Linear Algebra and its Applications,* 2nd Edition, Academic Press, NY, 1980, pp. 190-192.

Appendix – Structure of the feedback matrix

Matrix $\mathbf{B}(n;r,\phi)$ presented in (28) is composed by two null matrices and two square sparse matrices having a multi-diagonal structure, as follows:

$$\mathbf{B} = \begin{bmatrix} \mathbf{B_{11}} & \mathbf{B_{22}} \\ \mathbf{0} & \mathbf{0} \end{bmatrix}$$

$$\mathbf{B_{11}} = \begin{bmatrix}
\cdots & \ddots & \cdots & \ddots & \cdots & \ddots & \cdots & \ddots & \cdots & \ddots & \cdots & \ddots & \cdots & & \\
\ddots & \cdots & \frac{1}{3}s_{3\phi} & \cdots & s_{\phi} & \cdots & 0 & \cdots & s_{\phi} & \cdots & \frac{1}{3}s_{3\phi} & \cdots & \frac{1}{5}s_{5\phi} & \cdots & \\
\cdots & \frac{1}{5}s_{5\phi} & \cdots & \frac{1}{3}s_{3\phi} & \cdots & s_{\phi} & \cdots & 0 & \cdots & s_{\phi} & \cdots & \frac{1}{3}s_{3\phi} & \cdots & \frac{1}{5}s_{5\phi} & \cdots \\
 & \cdots & \frac{1}{5}s_{5\phi} & \cdots & \frac{1}{3}s_{3\phi} & \cdots & s_{\phi} & \cdots & 0 & \cdots & s_{\phi} & \cdots & \frac{1}{3}s_{3\phi} & \cdots & \ddots \\
 & & \cdots & \ddots & \cdots & \ddots & \cdots & \ddots & \cdots & \ddots & \cdots & \ddots & \cdots & \ddots & \cdots
\end{bmatrix}$$

$$\mathbf{B_{22}} = \begin{bmatrix}
 & & \cdots & \iddots & \cdots & \iddots & \cdots & \iddots & \cdots & \iddots & \cdots & \iddots & \cdots & \iddots & \cdots \\
 & \cdots & \frac{1}{5}c_{5\phi} & \cdots & \frac{1}{3}c_{3\phi} & \cdots & c_{\phi} & \cdots & 0 & \cdots & c_{\phi} & \cdots & \frac{1}{3}c_{3\phi} & \cdots & \iddots \\
\cdots & \frac{1}{5}c_{5\phi} & \cdots & \frac{1}{3}c_{3\phi} & \cdots & c_{\phi} & \cdots & 0 & \cdots & c_{\phi} & \cdots & \frac{1}{3}c_{3\phi} & \cdots & \frac{1}{5}c_{5\phi} & \cdots \\
\iddots & \cdots & \frac{1}{3}c_{3\phi} & \cdots & c_{\phi} & \cdots & 0 & \cdots & c_{\phi} & \cdots & \frac{1}{3}c_{3\phi} & \cdots & \frac{1}{5}c_{5\phi} & \cdots & \\
\cdots & \iddots & \cdots & \iddots & \cdots & \iddots & \cdots & \iddots & \cdots & \iddots & \cdots & \iddots & \cdots & &
\end{bmatrix}$$

where $s_{\vartheta} = sin\vartheta$ and $c_{\vartheta} = cos\vartheta$. The spacing between the diagonals (indicated by the horizontal dots) is filled with zeroes and determined by the controlled harmonic, r. The dimension of all matrix components is given by $N = n + p_{max}r$, where p_{max} is the number of terms retained in the complex Fourier series that describes the Smart Spring control function (9).